Neuron
Article

Axon Initial Segment Kv1 Channels Control Axonal Action Potential Waveform and Synaptic Efficacy

Maarten H.P. Kole,[1,2] Johannes J. Letzkus,[1,2] and Greg J. Stuart[1,*]
[1] Division of Neuroscience, John Curtin School of Medical Research, Australian National University, Canberra, ACT 0200, Australia
[2] These authors contributed equally to this work.
*Correspondence: greg.stuart@anu.edu.au
DOI 10.1016/j.neuron.2007.07.031

SUMMARY

Action potentials are binary signals that transmit information via their rate and temporal pattern. In this context, the axon is thought of as a transmission line, devoid of a role in neuronal computation. Here, we show a highly localized role of axonal Kv1 potassium channels in shaping the action potential waveform in the axon initial segment (AIS) of layer 5 pyramidal neurons independent of the soma. Cell-attached recordings revealed a 10-fold increase in Kv1 channel density over the first 50 μm of the AIS. Inactivation of AIS and proximal axonal Kv1 channels, as occurs during slow subthreshold somatodendritic depolarizations, led to a distance-dependent broadening of axonal action potentials, as well as an increase in synaptic strength at proximal axonal terminals. Thus, Kv1 channels are strategically positioned to integrate slow subthreshold signals, providing control of the presynaptic action potential waveform and synaptic coupling in local cortical circuits.

INTRODUCTION

Fast neuronal communication arises from the conversion of graded synaptic signals received at somatodendritic regions into all-or-none action potentials (APs) in the axon (Stuart et al., 1997). While traditionally APs are thought of as binary signals that transmit information about synaptic inputs via their rate and temporal pattern, there is now emerging evidence that both vertebrate and invertebrate axons can perform a more complex computational role (Debanne, 2004). Such axonal operations include frequency- and membrane potential-dependent propagation failure (Baccus, 1998; Debanne et al., 1997; Manor et al., 1991), as well as both short- and long-term broadening of the AP in the presynaptic terminal (Byrne and Kandel, 1996; Geiger and Jonas, 2000; Jackson et al., 1991). More recent evidence indicates that subthreshold somatodendritic voltage changes, evoked by excitatory postsynaptic potentials (EPSPs) or cortical up-states, can also be transmitted via the axon and are able to modulate transmitter release at synaptic terminals (Alle and Geiger, 2006; Shu et al., 2006b).

The axonal mechanisms underlying the ability of subthreshold somatodendritic voltage changes to modulate transmitter release are not well understood. Changes in presynaptic membrane potential could either influence the availability of presynaptic Ca^{2+} channels for activation or the AP waveform itself, both of which would be expected to influence presynaptic Ca^{2+} influx (Borst and Sakmann, 1999; Geiger and Jonas, 2000). Subthreshold depolarizations have been shown to increase the duration of APs in neocortical axons (Shu et al., 2006b, 2007), although not in hippocampal terminals (Alle and Geiger, 2006). However, depolarization has also been reported to decrease axonal AP amplitude (Shu et al., 2006b), which would be expected to decrease transmitter release (Bischofberger et al., 2002).

Subthreshold depolarizations may influence axonal K^+ channels. Axons contain a variety of voltage-gated K^+ (Kv) channels that can shape the axonal AP waveform. In particular, Kv1 channels are known to be densely clustered at subdomains of the axon, such as the distal region of the axon initial segment (AIS) (Inda et al., 2006; Van Wart et al., 2007), in juxtaparanodal regions of nodes of Ranvier (see Rasband and Shrager, 2000), as well as in synaptic nerve terminals (Geiger and Jonas, 2000; Southan and Robertson, 1998). Whereas juxtaparanodal Kv1 channels presumably contribute to reducing re-excitation of the node (Chiu and Ritchie, 1981), Kv1 channels in axon terminals are likely to influence presynaptic AP waveform and thereby transmitter release (Byrne and Kandel, 1996; Geiger and Jonas, 2000; Jackson et al., 1991; Shu et al., 2007). At present, the role of Kv1 channels in the axon initial segment is unknown.

Here, we directly investigate the properties and distribution of voltage-activated K^+ channels in the AIS and axon proper of neocortical layer 5 pyramidal neurons, as well as their role in controlling axonal AP waveform and intracortical synaptic transmission. We demonstrate that (1) AP repolarization in the AIS and axon proper is regulated independent of the somatic AP waveform, (2) this compartmentalization is due to a 10-fold increase in density of slowly inactivating Kv1 channels in the AIS, and (3)

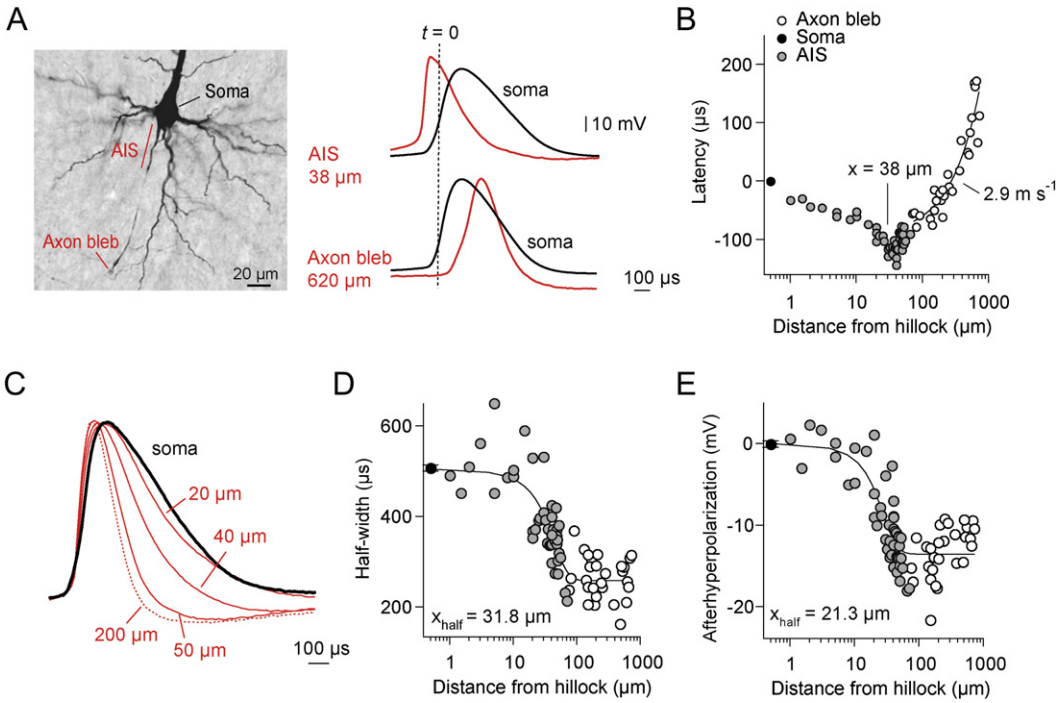

Figure 1. Site-Dependent Characteristics of Action Potential Properties in the Soma, Axon Initial Segment, and Axon Proper

(A) (Left) Photograph of a biocytin-filled layer 5 neuron indicating the soma, the unmyelinated AIS, a myelinated axonal region, and an axon bleb site accessible for whole-cell recording. (Right, top) Example traces show APs evoked by somatic current injection and recorded at the AIS 38 μm from the axon hillock (red) and at the soma (black). (Bottom) Example traces for an axon bleb recording 620 μm from the hillock. The $t = 0$ marks time of onset of the somatic AP.

(B) Plot of AP latency relative to that of the somatic AP (black) for APs recorded in the AIS (gray circles, n = 45) and axon blebs (open circles, n = 22) versus recording distance from the axon hillock. Minimum onset latency occurs ~38 μm from the axon hillock, which is slightly before the end of the AIS (45–70 μm). Linear fit to the axon bleb data yielded a conduction velocity of 2.9 m s^{-1}.

(C) Traces show APs recorded from the soma (black) and at the indicated axonal distances from the axon hillock (red). Recordings were obtained from different axons and for illustration baselined at AP threshold, scaled to the same amplitude and overlaid.

(D) Plot of axonal AP width at half-amplitude (half-width) versus recording distance from the axon hillock. The average somatic half-width is indicated in black. Data fitted with a sigmoid function yielding a half-maximum distance of 31.8 μm.

(E) Plot of axonal AP afterhyperpolarization amplitude (measured from AP threshold) versus recording distance from the axon hillock. The average somatic AHP is shown in black. Data fitted with a sigmoid function with a half-maximum distance of 21.3 μm.

Data are mean ± SEM.

inactivation of Kv1 channels in the AIS and proximal axon during steady-state somatodendritic depolarization or slow rhythmic oscillations generates a distance-dependent broadening of the axonal AP waveform, leading to facilitation of transmitter release at proximally located synaptic terminals.

RESULTS

Axonal Action Potential Properties

We first examined the spatial and temporal properties of axonal APs in large layer 5 pyramidal neurons. These neurons give rise to an axon initial segment of relatively large diameter (1–2 μm), with an unmyelinated region extending ~50 μm from the axon hillock (Sloper and Powell, 1979). While the myelinated axon beyond the AIS does not allow direct patch-clamp recording, in many instances axonal end-bulbs, recently called "blebs" (Shu et al., 2006b), appear due to the slice cutting procedure, and unmyelinated blebs are accessible to whole-cell recording. To allow comparison of somatic and axonal AP waveforms, we made dual whole-cell current-clamp recordings from the soma and AIS (1–65 μm from the hillock; n = 35) or the soma and axon blebs (25–720 μm from the hillock; n = 41, Figure 1A). Action potential properties during recordings from axon blebs were similar to those obtained during recordings directly from the AIS at comparable distances from the axon hillock (see Figure S1 in the Supplemental Data available with this article online).

APs were induced by brief somatic current injections from the resting potential (soma, −75.9 ± 0.4 mV; axon, −76.3 ± 0.4 mV; $p > 0.05$, n = 63). Figure 1 shows the spatial dependence of AP properties in the axon compared to the soma. The shortest axonal AP onset latencies occurred at a recording site 38 μm from the axon hillock, on average ~120 μs before AP onset at the soma (Figures

1A and 1B; n = 68). This finding is consistent with previous work in cortical pyramidal neuron axons (Palmer and Stuart, 2006; Shu et al., 2006a). A linear fit of onset latency in the axon proper (recordings >70 μm from the axon hillock) versus distance indicated that after initiation APs propagate down the axon with an average orthodromic axonal conduction velocity of 2.9 m s^{-1} (Figure 1B, n = 29).

While the amplitude of somatic and axonal APs was similar (n = 65, paired t test, $p > 0.49$), the shape of APs in the axon altered dramatically over the 50 μm of the AIS (Figure 1C). The AP half-width decreased steeply with distance from the axon hillock, from on average 518 ± 20 μs (n = 11) in the proximal 15 μm of the AIS to 290 ± 18.8 μs (n = 8) in the most distal region of the AIS (Figure 1D; soma, 503 ± 7.4 μs, n = 65). The AP half-width in the distal AIS was similar to that in axon blebs up to 720 μm from the axon hillock (Figure 1D; 266 ± 8.5 μs, n = 29, $p > 0.25$). In addition to these changes in AP duration, we also observed a dramatic increase in the amplitude of the AP afterhyperpolarization (measured from AP threshold) with distance from the axon hillock, which was on average 13.1 ± 0.6 mV (n = 21) more hyperpolarized in the distal AIS compared to the soma (Figure 1E; n = 21; soma, −0.07 ± 0.40 mV; n = 73, $p < 0.0001$). The AP afterhyperpolarization amplitude in the axon proper was similar to that recorded in the distal AIS (Figure 1E; −13.4 mV ± 0.57, $p > 0.6$, n = 29). Together, these data show that the axonal AP waveform undergoes a dynamic change along the relatively short region of the AIS that is then maintained throughout the axonal arbor.

Kv1 Channels Are Expressed at High Densities in the Axon Initial Segment

The dramatic decrease in half-width and increase in afterhyperpolarization of axonal APs described above is presumably mediated by K^+ channels localized in the AIS and axon proper. We therefore directly investigated the distribution and properties of axonal K^+ channels in the AIS and in axon blebs using cell-attached, outside-out, and whole-cell recordings. Recordings were made under conditions where voltage-activated Na^+ channels, as well as slowly activating Kv7/KCNQ/M-currents, were blocked to isolate the fast-activating K^+ currents likely to be responsible for the observed changes in axonal AP waveform (see Experimental Procedures). Cell-attached recordings from the soma of layer 5 pyramidal neurons showed that positive voltage steps (to +45 mV) from a negative holding potential (−110 mV) evoked fast-activating and slow-inactivating K^+ currents of small amplitude (Figure 2A; average: 4.0 ± 1.2 pA, n = 10). In contrast, K^+ currents in recordings from the AIS were 5-fold larger in the proximal initial segment (Figure 2A; 19.1 ± 5.5 pA; 5–30 μm from the axon hillock; n = 14, $p > 0.05$) to 10-fold larger in the distal AIS (Figure 2A; 44.1 ± 8.8 pA; 35–55 μm from the axon hillock; n = 21, $p < 0.001$). Axonal blebs at more distal axonal sites also contained high densities of fast-activating and slow-inactivating K^+ currents (Figure 2A; 30.2 ± 6.0 pA; n = 14, $p < 0.01$). Inclusion of 50 ms prepulses to +30 mV to inactivate the A-type K^+ current (Bekkers, 2000) reduced the peak amplitude of axonal K^+ currents by less than 10% (9.5% ± 2.0% block, n = 5), suggesting that the vast majority of the fast-activating K^+ current in the AIS and axon proper is D-type (Storm, 1988).

To test this hypothesis, we made outside-out recordings from the AIS or axonal blebs and locally applied dendrotoxin-I (DTX-I), which selectively blocks Kv1.1, Kv1.2, and Kv1.6 homomeric channels (Harvey, 2001; Robertson et al., 1996; Stühmer et al., 1989). Local extracellular application of 500 nM DTX-I rapidly suppressed evoked K^+ currents by 74% ± 2.7% (Figure 2B; n = 7). Subtraction of the control current from the current obtained in the presence of DTX-I showed that the DTX-sensitive current accounts for the vast majority of the inactivating component of the axonal outward K^+ current. Similar results were obtained when DTX-I was included in the pipette solution during cell-attached recordings. Comparison of peak K^+ current in cell-attached recordings obtained sequentially at identical axonal sites indicated that inclusion of 100–200 nM DTX-I in the pipette solution reduced axonal K^+ current by on average 79% ± 7% (Figure 2B; $p < 0.05$, n = 4).

We next analyzed the voltage dependence of activation and inactivation of axonal K^+ currents using cell-attached and outside-out recordings from the distal AIS, as well as whole-cell recordings from axonal blebs. As results were similar for the different recording configurations, the data were pooled. Activation protocols indicated a negative half-activation midpoint of on average −23.7 ± 1.7 mV, with a slope of 12.3 (Figure 2C; 4 outside-out and 11 cell-attached patches). The midpoint of half-maximum inactivation was −44.9 ± 1.5 mV, with a slope factor of 12.1, indicating that axonal K^+ channels are fully available for activation at resting membrane potentials but will undergo substantial inactivation during depolarization (Figure 2C; 2 whole-cell recordings, 4 cell-attached patches). We examined the kinetics of inactivation during long duration (5 s) pulses. As shown in Figure 2D, the average time course of inactivation during a step to +45 mV was best described by a double-exponential decay. Similar time constants were found in both cell-attached (n = 7) and whole-cell recordings (n = 7) and were therefore pooled. On average, the initial rapid component of 227 ± 26 ms (35% amplitude) was followed by a significantly slower component of 3.6 ± 0.4 s (65%) (Figure 2D; n = 14). Similarly, the recovery from prolonged channel inactivation (after 10 s pulses to +35 mV) at resting membrane potentials (−75 mV) followed a double-exponential time course with rapid (246 ± 20 ms, 31%) and slow components (Figure 2E; 2.29 ± 0.4 s, 69%, n = 6 whole-cell recordings). Based on the kinetics, voltage-dependence, and pharmacology, we conclude that outward K^+ current in the AIS and axon proper of cortical layer 5 pyramidal neurons is composed of primarily (~75%) DTX-sensitive, slowly inactivating, and low-voltage-activated Kv1 channels, which are distributed in a nonuniform manner with the highest densities in the distal AIS.

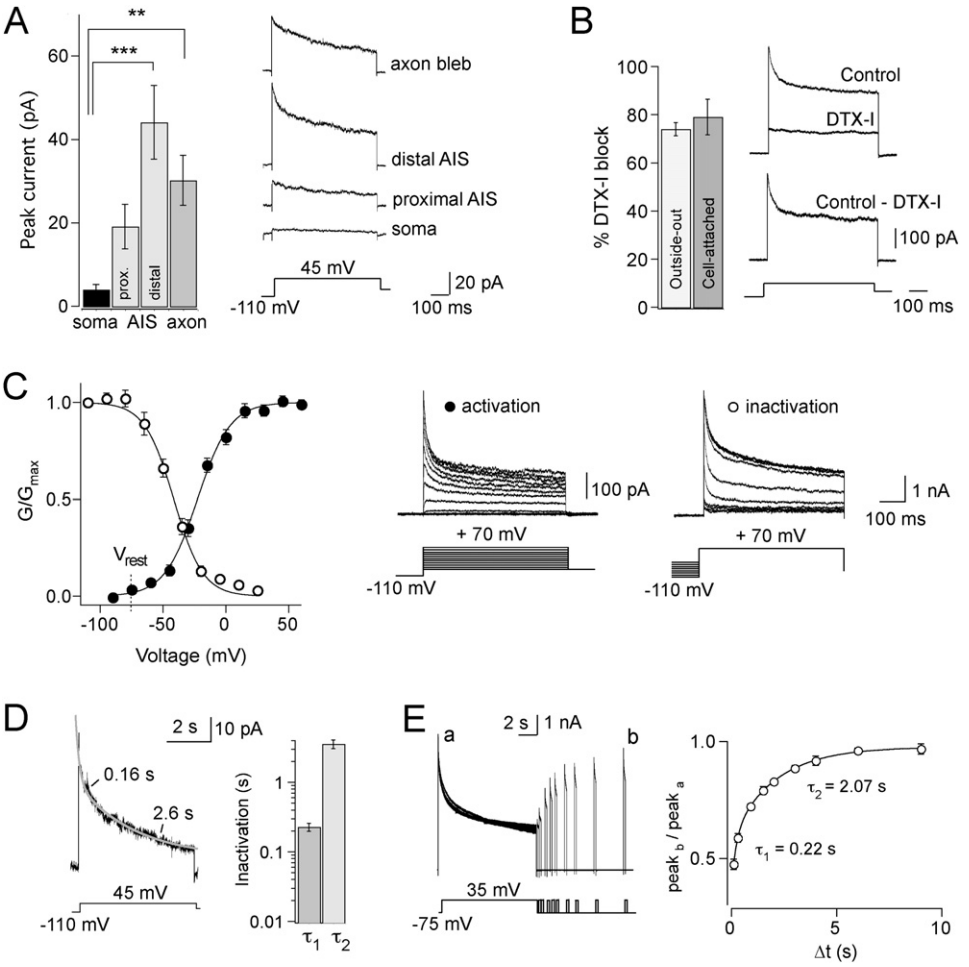

Figure 2. Distribution, Voltage Dependence, and Inactivation Properties of Cortical Axonal Kv1 Currents

(A) Mean amplitude of slowly inactivating K^+ currents evoked by voltage steps from −110 to +45 mV recorded in cell-attached patches from the soma, proximal AIS (5–30 μm from hillock), distal AIS (35–55 μm), and axonal sites (70–400 μm). Asterisks indicate significant increases in K^+ peak amplitudes compared to the soma (***$p < 0.001$ and **$p < 0.01$). Traces show examples of slow-inactivating K^+ current at the indicated locations (averages of four to six patches).

(B) (Right) Outside-out recordings of K^+ currents from AIS or axonal blebs before and after puffs with 500 nM DTX-I. Subtracted trace shows the DTX-sensitive current. Step protocol as in (A). Bars indicate the average current block in outside-out patches, or cell-attached configuration comparing different recordings from similar sites with and without DTX-I (100–200 nM).

(C) Activation (closed circles, n = 15) and steady-state inactivation (open circles, n = 6) of axonal K^+ currents. Inactivation was tested with 5 s inactivating prepulses. Lines represent Boltzmann fits yielding a half-activation midpoint of −24 mV and half-inactivation midpoint at −45 mV. V_{rest} indicates the average resting membrane potential.

(D) (Left) Example of the response to a 5 s voltage step (+45 mV) in cell-attached recordings. Trace is the average from five cells (three traces each). The time constants of inactivation were obtained from a double exponential fit (gray). (Right) Bar plot of the average time constants of inactivation (n = 14, pooled cell-attached and whole-cell recordings).

(E) (Left) Protocol and example of recovery from inactivation in whole-cell recordings from axon blebs following a 10 s prepulse to +35 mV. (Right) Summary plot of the mean normalized peak current amplitude (n = 6) evoked by test pulses at various latencies (b) after the control pulse (a). Line shows the double-exponential fit to the mean data with indicated time constants.

Data presented as mean ± SEM.

Kv1 Channels Selectively Control Axonal Action Potential Waveform

In order to determine whether the observed high density of axonal Kv1 channels (Figure 2) underlies the local control of AP waveform in the AIS and axon proper (Figures 1C–1E), we bath applied low concentrations of DTX-I during dual recordings from the soma and distal AIS or axon proper (Figure 3A; 40–200 μm from the axon hillock). Bath application of 50–100 nM DTX-I increased axonal AP half-width 2-fold (control, 374 ± 16 μs; DTX-I, 697 ± 46 μs; n = 5, $p < 0.01$), while causing only a small (4%) change in AP half-width at the soma (Figures 3A and 3B; control, 506 ± 14 μs; DTX-I, 524 ± 12 μs; $p < 0.05$). DTX-I also reduced the axonal afterhyperpolarization

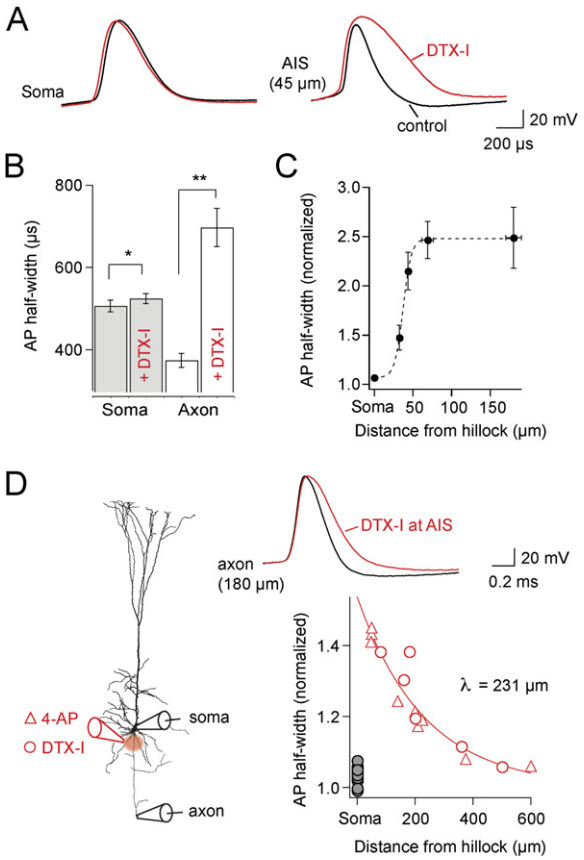

Figure 3. Kv1 Channels Control Axonal AP Repolarization

(A) Impact of bath application of 50–100 nM DTX-I on somatic (left) and axonal (right) APs before (black) and several minutes after DTX-I (red).

(B) Column plots of mean AP half-width (±SEM) pooled for recordings at the soma and between 40 and 180 μm from the axon hillock (n = 5). Asterisks indicate significant increases compared to control half-width for the axon and soma (**p < 0.01 and *p < 0.05, respectively).

(C) Pooled data (n = 12) illustrating the change in AP half-width versus recording distance from the axon hillock in the presence of DTX-I or identical experiments with 100 μM 4-AP. Data fitted with a sigmoid function with a half-maximum distance of ~37 μm.

(D) (Left) Schematic of the recording configuration for local application of 100 μM 4-AP or 500 nM DTX-I to the distal AIS (40–50 μm from the axon hillock) during dual whole-cell recording from soma and axon (open circles, DTX-I; triangles, 4-AP). (Right, top) Example of local DTX-induced axonal AP broadening recorded 180 μm from the axon hillock. (Right, bottom) Plot of AP half-width relative to control versus recording distance from the axon hillock. The axonal AP data (n = 13) were fitted with a single-exponential with a distance constant of 231 μm.

from −11.9 ± 2.2 mV to −3.2 ± 0.9 mV (n = 5, p < 0.01) and slightly increased axonal AP amplitude by 11% (control, 85.2 ± 2.6 mV; DTX-I, 93.0 ± 3.7 mV; n = 5, p < 0.05). Nearly identical observations were made following bath application of low concentrations (100 μM) of 4-aminopyridine (4-AP), which blocks Kv1 and Kv3 subfamilies of K^+ channels (Figure S2). The highly local nature of the Kv1-sensitive changes in axonal AP waveform is further demonstrated by plotting the DTX-I or 4-AP-induced increase in AP half-width versus recording distance from the axon hillock (Figure 3C). The data were well fitted by a sigmoid function, with the half-maximum change occurring in the AIS (37 μm from the axon hillock), similar to the observed spatial distribution of axonal AP half-width (Figure 1D) and Kv1 channel expression (Figure 2A). These observations suggest that the highly nonuniform Kv1 distribution in the AIS plays a critical role in controlling AP waveform in the AIS and axon proper. Furthermore, they indicate that local modulation of Kv1 channels in the AIS would be expected to influence axonal AP duration in the absence of any changes in somatic AP waveform.

To test this idea, we applied DTX-I (500 nM) or 4-AP (100 μM) to the distal AIS (40–50 μm from the hillock) during simultaneous recordings from the soma and axon at different distances from the axon hillock (Figure 3D). We estimate these local applications have an effective radius of less than 50 μm (Figure S3). The local block of AIS K^+ channels increased AP half-width at the site of application by 45% (Figure 3D; control, 376 μs ± 32 μs; local K^+ block, 544 ± 45 μs; n = 5, p < 0.05). This increase in AP width propagated down the axon, leading to ~20% broadening of axonal APs 140–210 μm from the axon hillock, decreasing to ~6% broadening at ~600 μm (Figure 3D; distance constant [λ] ~231 μm, n = 15). Thus, local modifications in AP duration at the AIS propagate orthodromically a significant distance down the axon.

Axonal Kv1 Channels Regulate Transmitter Release

We next investigated the impact of modulation of Kv1 channels on transmitter release using paired recordings from synaptically connected layer 5 pyramidal neurons (Figure 4A). Unitary excitatory postsynaptic potentials (uEPSPs) had a short latency (1.2 ± 0.08 ms; range 0.87 to 2 ms; n = 20) consistent with monosynaptic connections (Markram et al., 1997). After a baseline recording period of 10 min, bath application of DTX-I (75–100 nM) increased uEPSP amplitude ~2-fold (Figures 4A and 4B). On average, uEPSP amplitude increased from 0.64 ± 0.11 mV in control to 1.27 ± 0.23 mV in DTX-I (Figure 4B; p < 0.05, n = 7). This change in synapse strength was accompanied by a concomitant reduction in the paired-pulse ratio (PPR) (Figure 4C; control, 1.14 ± 0.10; DTX-I, 0.72 ± 0.04; p < 0.001, n = 7), suggesting a presynaptic site of DTX-I action. Furthermore, coefficient of variation (CV) analysis of uEPSP amplitude showed that all data points were located above or on the identity line, consistent with an exclusively presynaptic effect of bath application of DTX-I (Figure 4D). In keeping with this interpretation, somatic input resistance increased only slightly in DTX-I (~4%; control, 26 ± 2 MΩ; DTX-I, 27 ± 2 MΩ; p < 0.01). These data show that axonal Kv1 channels act presynaptically to suppress transmitter release and thereby exert a powerful inhibitory control over layer 5 uEPSP amplitude at intracortical synapses. We also observed a strong positive correlation between the extent of uEPSP enhancement after Kv1 channel block and the baseline

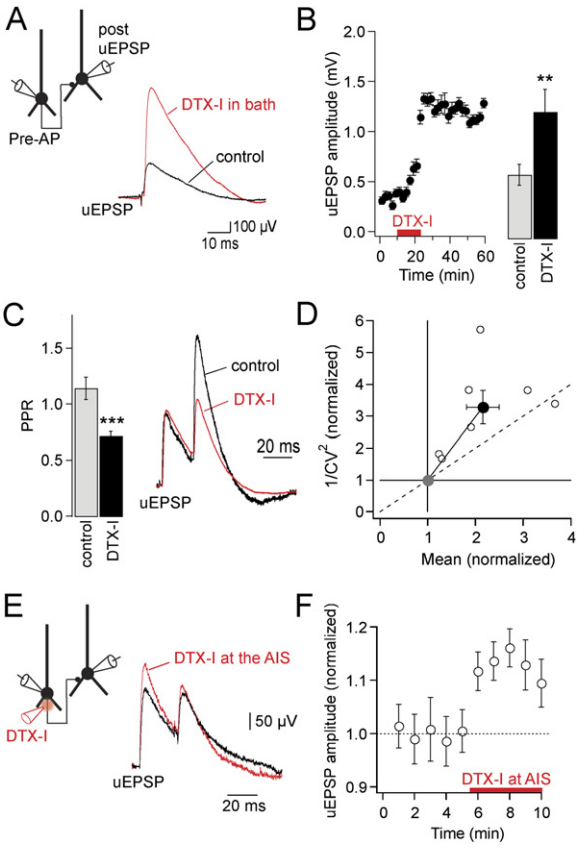

Figure 4. Kv1 Channels Influence Synaptic Transmitter Release

(A) (Left) Schematic of the experimental configuration for whole-cell paired recordings from synaptically connected layer 5 pyramidal neurons. (Right) Example of control uEPSP (black) and after bath application of 100 nM DTX-I (red; averages of 75 sweeps).

(B) (Left) Example time course of uEPSP enhancement after DTX-I application (same experiment as in [A]). (Right) Bar graph of pooled data for uEPSP amplitude before (control, gray) and after DTX-I application (black) shows on average a two-fold increase in uEPSP amplitude ($p < 0.05$; $n = 7$).

(C) Bar graph showing the reduction of paired-pulse ratio by DTX-I ($p < 0.001$; $n = 7$). (Inset) Example uEPSPs evoked by APs at a 25 ms interval normalized to the amplitude of the first uEPSP (same experiment as in [A] and [B]; average of >75 sweeps).

(D) Coefficient of variation (CV) analysis of the effect of bath application of DTX-I suggests an exclusively presynaptic action since all points are located above or on the identity line (dashed).

(E) Example uEPSPs during control (black) and local application of DTX-I (100–500 nM) to the distal AIS (red; averages 76 sweeps).

(F) Time course of average uEPSP facilitation following locally applied DTX-I ($n = 6$). DTX-I induced a 1.13-fold increase in the uEPSP amplitude ($p < 0.05$).

Data shown as mean ± SEM.

PPR (Figure S4; $r^2 = 0.73$; $p < 0.05$, $n = 7$), supporting the notion that axonal Kv1 channels play an important role in setting the release probability. These observations indicate that modulation of axonal Kv1 channels would be expected to have a direct and significant impact on synaptic efficacy at layer 5 to layer 5 synapses.

To test the role of Kv1 channels in the AIS, we locally applied DTX-I to the distal AIS of the presynaptic neuron (as in Figure 3D) during recordings from layer 5 pyramidal neuron pairs (Figure 4E). Local block of AIS Kv1 channels in the presynaptic neuron increased uEPSP amplitude on average 1.13 ± 0.05-fold (Figure 4F; $p < 0.05$, $n = 6$). This increase in uEPSP amplitude occurred in the absence of any change in pre- or postsynaptic somatic input resistance (98% ± 2% and 97% ± 3% of control, respectively, $p > 0.5$, $n = 6$ each). These results suggest that local broadening of action potentials in the AIS is able to enhance the strength of layer 5 to layer 5 synapses.

Modulation of Axonal Action Potential Waveform by Neuronal Activity

To what extent can the axonal AP waveform in the AIS and axon proper be regulated by neuronal activity? To examine this, we compared two well-characterized modes of activity in the somatosensory cortex: burst firing (Williams and Stuart, 1999) and slow oscillatory rhythms (Steriade et al., 1993). First, we evoked a short-lasting high-frequency burst of three APs at 200 Hz by somatic current injection during dual recordings from the soma and distal AIS or proximal axon (~50–160 µm from the hillock). As shown in Figure 5A, burst firing led to an immediate broadening of somatic APs by 1.7-fold (1.7 ± 0.03-fold increase between first and third AP, $p < 0.0001$, $n = 7$). In contrast, APs in the distal AIS and/or proximal axon maintained a constant half-width (1.04 ± 0.03-fold change, $p > 0.2$, $n = 7$). The slight reduction in somatic and axonal AP amplitude during high-frequency bursts (15% ± 2% and 21% ± 4%, respectively, $p > 0.13$, $n = 7$) is presumably due to Na^+ channel inactivation.

Next, we tested whether longer-lasting subthreshold activity as occurs during cortical up- and down-states (Steriade et al., 1993) influences the axonal AP waveform. To mimic slow cortical oscillations, depolarizing current injections were repetitively applied to the soma at 0.67 Hz, with amplitudes just subthreshold for AP firing (Figure 5B). APs in these experiments were generated by additional brief current injection at the end of up- and down-states. These experiments indicated that axonal APs (45–150 µm from the hillock) were significantly increased in half-width during up-states by on average 1.4-fold (Figure 5B; 1.39 ± 0.06, 20th/1st AP half-width, $p < 0.001$, $n = 7$), with a much smaller increase observed during the down-state (1.09 ± 0.02, $p > 0.16$, 20th/1st AP half-width). No further changes in axonal AP half-width were observed in longer-duration recordings (up to ~2 min). These changes were specific for axonal APs, as the somatic AP half-width remained constant during up- and down-state (1.06- and 0.99-fold, 20th/1st AP, respectively, $p > 0.08$ and $p > 0.7$, $n = 7$). Thus, unlike somatic APs, which broaden rapidly during high-frequency AP bursts, axonal AP duration is selectively increased during sustained subthreshold activity, consistent with the properties of slow-inactivating Kv1 channels in the AIS. Furthermore, these data suggest that somatic and axonal

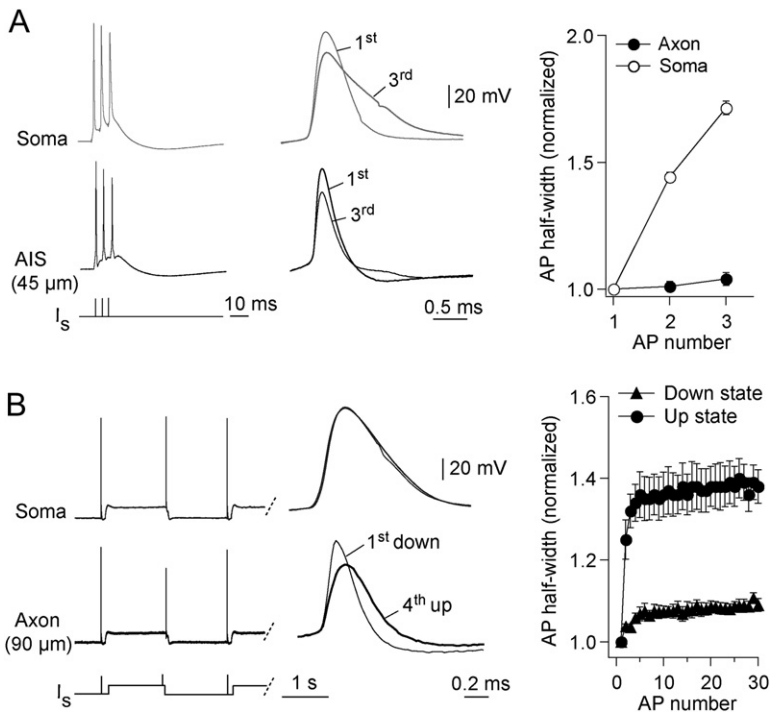

Figure 5. Differential Modulation of Somatic and Axonal AP Width by Neuronal Firing Patterns

(A) (Left) Example of a dual whole-cell recording from soma (top) and axon initial segment (bottom). A 200 Hz burst of three APs was induced by somatic current injection (I_s, bottom protocol). (Middle) Expanded view of overlaid first and third AP in the burst. (Right) Summary plot of mean AP duration versus number during the burst. Whereas the somatic AP half-width increased significantly ($p < 0.001$), the axonal AP half-width was unaffected ($p > 0.2$, $n = 7$).

(B) (Left) Slow rhythmic oscillations mimicking up- and down-states were induced by repetitive subthreshold 1.5 s depolarizations generated by ~300 pA somatic current injections (I_s, bottom protocol). At the end of each up- or down-state, APs were evoked by an additional brief current injection (2 nA, 3 ms). (Middle) Overlaid APs showing the fourth AP during the up-state compared to the control AP (first of down-state). (Right) Average broadening of axonal APs during the up- (circle) or down-states (triangle), plotted versus AP number. Data are mean ± SEM ($n = 6$).

domains integrate neuronal activity in a highly compartmentalized and independent fashion.

Properties of Axonal Action Potential Modulation by Subthreshold Depolarizations

If the properties of axonal Kv1 channels are responsible for the observed changes in axonal AP waveform during subthreshold depolarizations, the time course of axonal AP broadening (and recovery from broadening) should have similar kinetics to inactivation (and recovery from inactivation) of Kv1 channels. To characterize the kinetics of axonal AP broadening, we induced APs at specific time points after just subthreshold, steady-state depolarization of the soma (Figure 6A; average, 10.1 ± 0.9 mV, $n = 8$). APs were elicited at 500 ms intervals up to 9.5 s after the onset of somatic depolarization and their half-width expressed as a ratio of the AP duration in the absence of depolarization. As shown in Figure 6A, somatic depolarization leads to a time-dependent broadening of axonal APs by up to 1.40 ± 0.02-fold (recording location: 40–200 µm from the axon hillock; $p < 0.001$, $n = 8$), as well as a reduction in the AP afterhyperpolarization from −9.3 ± 0.3 to −7.9 ± 0.2 mV ($p < 0.001$, $n = 7$). In addition to this increase in axonal AP duration, the voltage-time integral of the axonal AP waveform was increased by ~15% (from 24.8 to 28.4 µV.s, $p < 0.01$, $n = 7$) despite a small reduction in axonal AP amplitude (12% ± 4% decrease at 9.5 s, $p < 0.05$, $n = 7$). Axonal AP broadening could be fitted with a double exponential function with time constants of 160 ms (22%) and 3.8 s (78%) (Figure 6A). Recovery from axonal AP broadening determined after a 10 s depolarization had both fast and slow components with time constants of 96 ms (48%) and 2.4 s (52%), respectively (Figure 6B; $n = 7$). To obtain more conclusive evidence about the contribution of Kv1 channel inactivation, we tested the impact of low concentrations of 4-AP on the depolarization-induced axonal AP changes. Bath application of 4-AP (100 µM) blocked the increase in axonal AP half-width observed during steady-state depolarization (Figure 6C; 1.05 ± 0.04-fold increase at 9.5 s, $n = 4$, $p < 0.0001$). In comparison, the somatic AP showed only a minor change in half-width (Figure 6C; 1.05 ± 0.01-fold broadening at 9.5 s, $p > 0.22$, $n = 8$), which was also blocked by 4-AP (1.0 ± 0.01-fold, $p < 0.05$, $n = 4$). These data strongly indicate that steady-state inactivation of axonal Kv1 channels is responsible for axonal AP broadening during subthreshold somatodendritic depolarizations.

How far does this axonal AP broadening propagate down the axon? We investigated this by recording the impact of somatic depolarization on axonal AP waveform in axonal recordings up to 720 µm from the axon hillock (Figure 6D, $n = 20$). These data indicate that axonal AP broadening decreases exponentially with distance from the soma with a distance constant (λ) of 675 µm and can be significant as far as 500–600 µm from the axon hillock (broadening: 1.2 ± 0.04-fold, $p < 0.05$, location: 480–650 µm, $n = 5$). This finding shows that axonal AP broadening is more effectively propagated down the axon during steady-state depolarization than following local 4-AP/DTX applications to the AIS (Figure 3D). This is presumably the case because the passively spreading somatic depolarization leads to inactivation of axonal Kv1 channels at

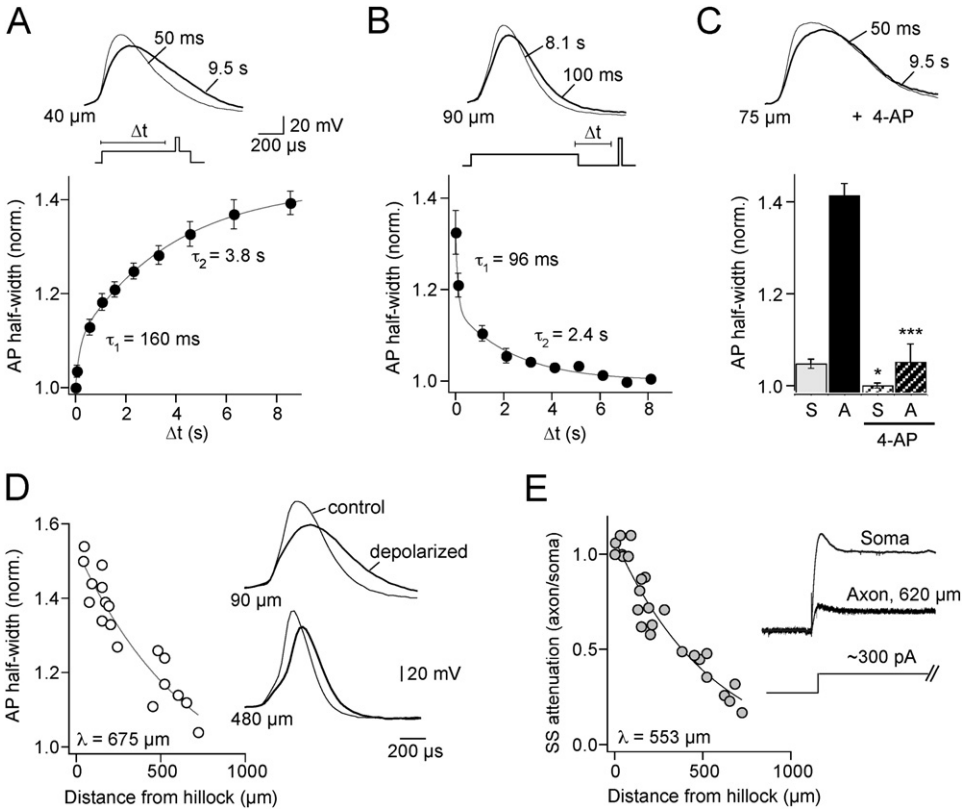

Figure 6. Temporal and Spatial Properties of Kv1 Channel-Dependent Axonal AP Broadening

(A) Action potentials (APs) recorded in the distal AIS at the early onset (50 ms, thin) and end (9.5 s, thick) of subthreshold depolarization (~10 mV depolarized from rest) generated by somatic current injection. Step protocol shown at the bottom. Mean data on axonal AP half-width (n = 8) versus latency (Δt) could be fitted with a double exponential function (line) with indicated time constants.

(B) Recovery of axonal AP broadening at resting membrane potentials investigated at latencies (Δt) between 100 ms and 8.1 s following a 10 s depolarizing prepulse (~10 mV). Mean data (n = 7) were plotted and fitted with a double exponential function (line) with indicated time constants.

(C) (Top) Example of bath application of 100 µM 4-AP, which removed time-dependent axonal AP broadening during subthreshold depolarizations (thick). Columns indicate the average broadening at 9.5 s for the somatic (S) and axonal (A) AP with and without 100 µM 4-AP. Both somatic and axonal AP broadening was significantly reduced in 4-AP ($p < 0.05$ and $p < 0.001$, respectively, n = 4).

(D) Plot of average subthreshold depolarization-induced AP broadening versus the distance of the axonal recording site from the axon hillock. Data fitted with a single exponential with a distance constant (λ) of 675 µm. (Right) Examples of axonal APs at the indicated locations at resting membrane potentials (control) and following subthreshold depolarizations.

(E) Long subthreshold depolarizations (10 s, ~300 pA) applied to the soma during simultaneous somatic (thin) and axonal (thick) whole-cell recordings. Plot of axosomatic steady-state attenuation (based on voltage integral, n = 24) versus distance of the axonal recording site from the axon hillock. Data fitted with a single-exponential yielding an apparent length constant of 553 µm.

Data represent mean ± SEM.

distal axonal sites. Consistent with this idea, steady-state voltage attenuation in layer 5 axons could be fit with a single exponential with a distance constant of 553 µm (Figure 6E, n = 24), similar to that observed for AP broadening.

Depolarization-Induced Inactivation of Axonal Kv1 Channels Facilitates Transmitter Release at Proximal Synapses

We next investigated whether the observed Kv1 channel-dependent AP broadening during subthreshold depolarizations influences synaptic efficacy in paired recordings between synaptically connected layer 5 pyramidal neurons. The presynaptic neuron was depolarized to potentials just subthreshold for AP firing (Figure 7A; average, 12.7 ± 0.4 mV; n = 32) and APs elicited by additional, brief current injections 75 ms, 2 s, and 8 s after depolarization onset. This regime was interleaved with episodes with identical AP pattern but without steady-state somatic depolarization. These experiments revealed a significant enhancement of uEPSP amplitude in ~56% of the tested pairs (18/32) (cf. Shu et al., 2006b). In pairs that showed a significant effect, uEPSP facilitation developed slowly: there was no effect after 75 ms of depolarization (99% ± 1%; $p > 0.10$), but a highly significant increase after 2 s (104% ± 1%; $p < 0.001$), which developed further at 8 s (Figure 7B; 110% ± 1%; $p < 0.001$). These data indicate

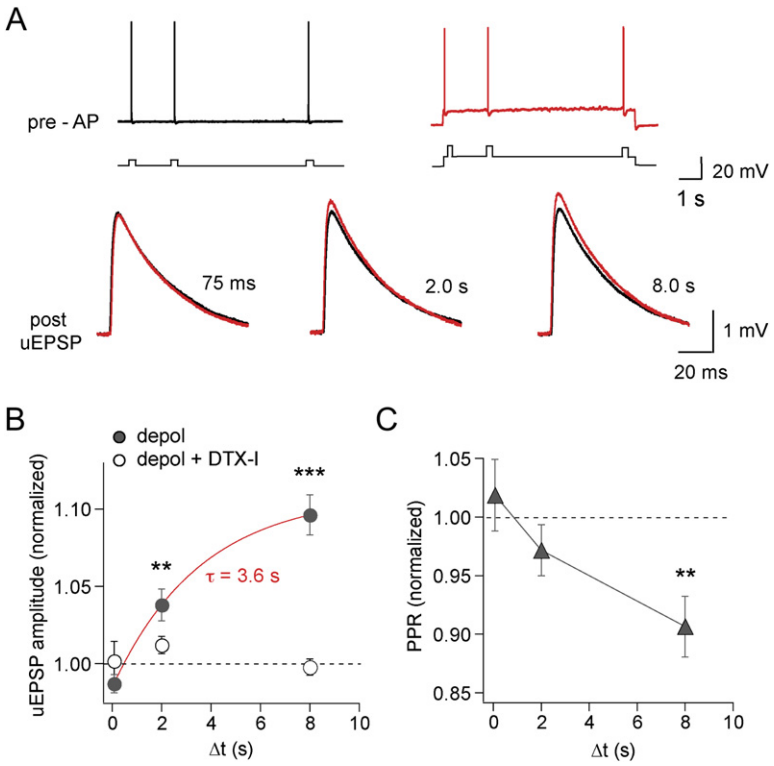

Figure 7. Facilitation of Synaptic Release during Subthreshold Depolarizations Is Mediated by Inactivation of Axonal Kv1 Channels

(A) (Top) Protocol used to assess synapse efficacy in paired recordings between synaptically connected layer 5 pyramidal neurons without (left, black) or with presynaptic subthreshold depolarization (right, red). Episodes with and without subthreshold depolarization were interleaved and the effect of subthreshold depolarization characterized by comparing uEPSP amplitude at the corresponding time points. (Bottom) Example uEPSPs evoked in the absence (black) or presence of presynaptic subthreshold depolarization (red) at the indicated time points (averages of ~100 sweeps).

(B) Plot of average uEPSP amplitude versus time after the onset of presynaptic subthreshold depolarization relative to uEPSP amplitude in the absence of somatic depolarization (gray circles; n = 18) shows significant facilitation after 2 s and 8 s of depolarization. These data were fitted with a single exponential with the indicated time constant. Bath application of 75–100 nM DTX-I completely abolished uEPSP enhancement (open circles; $p < 0.001$; n = 6).

(C) Facilitation of uEPSPs was accompanied by a concomitant reduction in paired-pulse ratio, consistent with an enhancement of release probability by somatic depolarization. Asterisks indicate significant difference.

Data plotted as mean ± SEM.

that subthreshold somatodendritic depolarizations significantly increase the strength of layer 5 synapses in a graded manner depending on the duration of the preceding depolarization.

What mechanism underlies this facilitation? The time course of uEPSP enhancement was fit by a single exponential with a time constant of 3.6 s (Figure 7B). This time course is in the same range as the slow time constant of depolarization-induced axonal AP broadening ($\tau = 3.8$ s; compare Figure 7B and Figure 6A), suggesting a similar underlying mechanism. To test this, we investigated the impact of bath application of DTX-I. Application of DTX-I (75–100 nM) completely blocked uEPSP facilitation during subthreshold somatic depolarization of the presynaptic neuron (Figure 7B; 100% ± 1% at 8 s; $p < 0.001$; n = 6). Consistent with a presynaptic locus, uEPSP facilitation was associated with a time-dependent reduction in the paired-pulse ratio (Figure 7C, 91% ± 3% of control at 8 s; $p < 0.01$; n = 18). Taken together, these results suggest that somatic depolarization of the presynaptic neuron acts via inactivation of Kv1 channels to increase axonal AP duration and thereby enhance transmitter release at layer 5 synapses.

One possible explanation for the wide range of uEPSP facilitation during subtreshold depolarizations (4% to 24% increase, with 44% of pairs showing no facilitation) is that presynaptic terminals are spatially distributed and thereby differentially influenced by somatodendritic depolarization (see Figure 6D). This hypothesis was tested by correlating the effect of steady-state depolarization on uEPSP amplitude with the location of putative synaptic contacts identified after filling pre- and postsynaptic neurons with biocytin and subsequent 3D reconstruction (Figure 8A). In five pairs, putative synapses could be successfully resolved (see Figure 8B), with each pair having two to six contacts primarily on basal dendrites (89%). Putative contacts were detected on a diverse range of collateral branches (first to fifth order, on average 3.11 ± 0.31, n = 18 synapses), which terminated predominantly on second or third order basal dendrites (2.17 ± 0.19, n = 18). The average soma-to-synapse path length for axonal (232.8 ± 22.7 μm, range: 87–385 μm) and dendritic arbors (71.1 ± 8.0 μm, n = 18) were in close agreement with previous morphometric analyses (Markram et al., 1997). To analyze the relationship between synapse location and facilitation, for each connected pair the increase in uEPSP amplitude (Figure 8C) was plotted against the average axonal path length to the synapse. The results indicate a negative correlation between the average soma to terminal bouton distance and the degree of uEPSP facilitation (Figure 8D; $r^2 = 0.93$; $p < 0.007$, n = 5). Similarly, the average axonal branch order was significantly and negatively related to uEPSP facilitation ($r^2 = 0.875$, $p < 0.02$). In contrast, the average dendritic geometrical path length, from synapse to soma, was not related to facilitation ($r^2 < 0.01$, n = 5). These data strongly indicate that the distance of

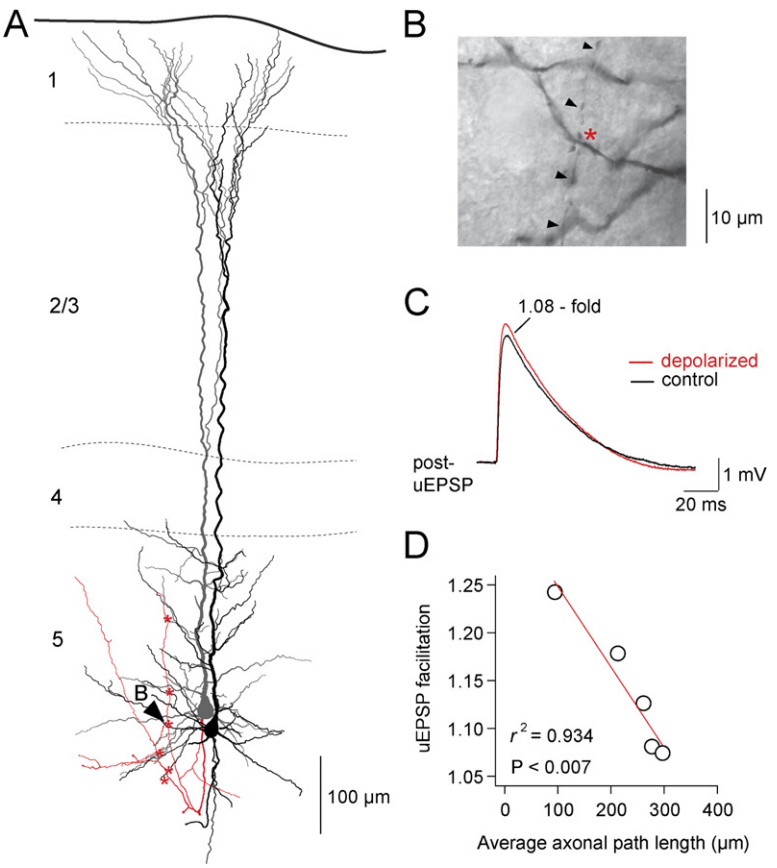

Figure 8. Depolarization-Induced uEPSP Facilitation Targets Proximal Synaptic Terminals

(A) 3D morphological reconstruction of a connected layer 5 pair with the presynaptic soma and dendrites (gray), presynaptic axon (red), and postsynaptic soma and dendrites (black). Red asterisks mark putative synaptic sites, with synapse B (arrow) shown in panel (B).

(B) Identification of a putative synaptic contact by close apposition of the axon and dendrite in a similar focal plane indicated by the presence of pre- or postsynaptic swellings (red asterisk). Black arrowheads indicate the path of the axon collateral.

(C) Example of the uEPSP of the same pair evoked from resting potential (black) and after 8 s depolarization (red, averages of 80 trials), showing a significant 1.08-fold increase in peak amplitude.

(D) Plot of the average axonal path length from the axon hillock to putative synapse terminals versus uEPSP facilitation after 8 s subthreshold depolarization showing a highly significant negative correlation. Red line indicates a linear regression fit to the data (n = 5). Each data point represents the average of two to six synaptic contacts.

boutons from the soma and AIS plays an important role in determining the extent of subthreshold modulation of intracortical synaptic strength.

DISCUSSION

The present study provides a detailed investigation of the properties, distribution, and function of voltage-activated K^+ channels in the axon initial segment. These data reveal that Kv1 channels, present at high densities in the distal AIS and axon proper, play a dynamic role in shaping the orthodromic AP. The electrotonic proximity of the AIS to the soma combined with the inactivation properties of Kv1 channels allows somatodendritic depolarizations to control axonal AP waveform in a distance-dependent fashion, which can have a significant impact on transmitter release at synaptic terminals close to the soma.

Role of the Axon Initial Segment

The AIS defines the initial unmyelinated region of the axon (Sloper and Powell, 1979) that contains the site of AP initiation in cortical pyramidal neurons (Palmer and Stuart, 2006; Shu et al., 2006a). We now describe that the AIS also plays a key role in the regulation of the axonal AP waveform independent of the soma. This remarkable functional compartmentalization is likely to come about for a number of reasons. First, as we show, the high density of DTX-sensitive Kv1 channels in the distal AIS (Figure 2) shortens the local axonal AP to a very brief pulse of ~260 µs (at 34°C), comparable to previously recorded presynaptic action potentials (Alle and Geiger, 2006; Borst and Sakmann, 1999; Dodson et al., 2003; Geiger and Jonas, 2000; Jackson et al., 1991). Second, the large capacitance of the soma limits invasion of axonal APs. Finally, following invasion of the soma by the initial segment spike, repolarization of the somatodendritic AP is mediated almost exclusively by activation of DTX-insensitive K^+ channels, which must be located at high densities at somatic and proximal dendritic regions. Consistent with this idea, recent data indicate that K^+ channels at the soma and proximal dendrites of cortical pyramidal neurons are largely DTX insensitive (Bekkers and Delaney, 2001; Guan et al., 2006) and present at densities significantly higher than previously thought (Schaefer et al., 2007).

Cortical Axon K^+ Channel Type and Distribution

We observed a slowly inactivating outward K^+ current with ~10-fold higher densities in the distal AIS compared to the soma, composed primarily (~75%) of DTX-sensitive Kv1 channels. The finding that axons contain a high density of Kv1 channels is consistent with recent data from layer 5 pyramidal neurons in prefrontal cortex (Shu et al.,

2007) and from other myelinated and unmyelinated axons and axon terminals (Dodson et al., 2003; Geiger and Jonas, 2000; Weller et al., 1985; Wolff et al., 1998). What is the precise subunit composition of Kv1 channels in the AIS and axon proper of cortical pyramidal neurons? The α subunits Kv1.1, Kv1.2, Kv1.3, and Kv1.4 are all abundantly expressed in neocortical pyramidal neurons (Guan et al., 2006). Recent data indicate that axonal K^+ current in cortical pyramidal neurons is mediated primarily by Kv1.2 based on block by the Kv1.2 toxin rTityustoxin-Kα, with only a minimal contribution of Kv1.1 (Shu et al., 2007). Based on kinetics, coassembly of Kv1.2 and Kv1.4 as heteromultimers may underlie the fast- and slow-inactivating components of the observed axonal K^+ current (Stühmer et al., 1989). These data suggest that Kv1.2 α subunits, either as homomers or as heteromultimeric channels with Kv1.4, or in association with Kvβ2-subunits, make up the dominant component of axonal K^+ conductance in cortical pyramidal neurons. Although the cellular mechanism controlling the clustering of voltage-gated K^+ channels in the AIS region is not well understood, recent work shows that the protein Caspr2 is expressed in the distal end of the AIS and colocalizes precisely with Kv1.2 α subunits (Inda et al., 2006). A similar interaction is found at nodes of ranvier (Rasband and Shrager, 2000; Rasband et al., 1998), suggesting possible similarities in the molecular organization of Kv1 channels in axonal nodes and initial segments.

Impact of Kv1 Channels on Axonal Action Potential Waveform and Synaptic Transmission

Our results show that Kv1 channels are available in high densities and with activation kinetics fast enough to play a critical role in repolarization of axonal APs with minimal impact on somatic AP repolarization. Two implications follow from these findings. First, by shortening the duration of cortical axonal APs, as well as increasing the amplitude of the afterhyperpolarization, the high density of Kv1 channels in the AIS and the axon proper will act to increase the fidelity of axonal AP propagation during high-frequency AP firing. Indeed, short bursts of APs (at 200 Hz) had no impact on axonal AP repolarization (Figure 5), and consistent with this, previous data indicate that AP propagation in cortical axons is reliable, even during high-frequency AP bursts (Cox et al., 2000; Koester and Sakmann, 2000; Williams and Stuart, 1999). In contrast, Kv1 channels at the terminal boutons of the calyx of Held activate too slowly to influence AP duration and are thought to rather play a role in dampening nerve terminal excitability during sustained depolarizations (Dodson et al., 2003; Dodson and Forsythe, 2004; Ishikawa et al., 2003).

A second important finding in our study is that the ability of slow subthreshold somatodendritic voltage changes to modulate transmitter release arises from Kv1 channel inactivation properties. Analysis of steady-state inactivation indicates that a 10 mV depolarization from the resting membrane potential would be expected to inactivate ~10% of the available Kv1 channels (Figure 2). The reduced availability of Kv1 channels during subthreshold somatodendritic depolarization leads to broadening of axonal APs up to ~1.4-fold (Figures 5 and 6). The conclusion that inactivation of Kv1 channels underlies axonal AP broadening is consistent with recent work in prefrontal cortex (Shu et al., 2007). Two independent lines of evidence suggest a causal relationship between broadening of axonal APs and enhancement of synaptic transmission by steady-state depolarization: both phenomena displayed a very similar time dependence (τ_{slow} = 3.8 s and τ = 3.6 s, respectively; Figures 6 and 7) and were abolished completely by pharmacological block with DTX-I. In addition, global or local pharmacological block of Kv1 channels was found to cause both AP broadening and uEPSP facilitation (Figures 3 and 4). The effect of AP broadening on synaptic transmission is likely to be via an increase in release probability, since uEPSP facilitation was associated with a reduction in PPR, and coefficient of variation analysis indicated that the locus of DTX-I action was exclusively presynaptic. Taken together, these results suggest that axonal APs broadened locally at the AIS and proximal axon ultimately invade axon terminals to enhance transmitter release.

The ability of locally broadened axonal APs to propagate throughout large regions of the axonal arbor of cortical layer 5 pyramidal neurons is due in part to the long apparent length constant of these axons (553 μm; Figure 6E). This value is slightly longer than previous estimates in unmyelinated axons (Alle and Geiger, 2006; Shu et al., 2006b) (430 and 417 μm, respectively), but similar to estimations using cable analysis of axons in the posterior pituitary (510 μm; Jackson, 1993). Theoretically, the long axonal length constant could mean that somatodendritic depolarizations are transmitted all the way to nerve terminals and influence transmitter release by affecting the availability of voltage-activated Ca^{2+} channels or by raising resting Ca^{2+} levels in synaptic terminals (Awatramani et al., 2005). Indeed, the addition of Ca^{2+} buffers partially blocks facilitation of synaptic release in unmyelinated cortical axons during subthreshold depolarization (Alle and Geiger, 2006; Shu et al., 2006b). In contrast, in the axons examined in our study, bath application of DTX-I completely abolished facilitation of transmitter release during subthreshold somatic depolarization of the presynaptic neuron (Figure 7B), indicating that somatodendritic control of release depends solely on modulation of axonal Kv1 channels. These data suggest that multiple, perhaps cell-specific, mechanisms may exist for translating subthreshold somatodendritic voltage changes into changes in transmitter release at the synapse. Furthermore, while our data do not rule out a role of modulation of Kv1 channels in the presynaptic bouton, the extent of axonal AP broadening and uEPSP facilitation during local DTX-I application to the AIS was similar in magnitude to that observed during subthreshold depolarizations, consistent with the idea that inactivation of Kv1 channels in the AIS during subthreshold depolarizations is sufficient to account for the observed facilitation of uEPSPs.

In addition to cell specificity, our data indicate that synapse location in the axonal arbor influences the ability of somatic steady-state depolarizations to enhance uEPSP amplitude (Figure 8), with this effect being greatest for the most proximal synapses. This is consistent with the observed attenuation of AP broadening with distance (Figure 6D) and can presumably explain why a significant number of layer 5 pairs did not display uEPSP facilitation (see also Shu et al., 2006b). These data suggest that, in addition to the well-characterized importance of synapse location in the dendritic tree (Williams and Stuart, 2003), synapse location in the axonal arbor can have an unprecedented and profound impact on signal processing.

Physiological Relevance

The present data indicate a new functional role of the AIS. In addition to AP initiation (Palmer and Stuart, 2006; Shu et al., 2006a) and precise timing (Kuba et al., 2006), we now show that the AIS is critical for regulating the duration of the presynaptic axonal AP waveform and thereby controlling release probability at intracortical synapses. Under which conditions is this phenomenon likely to influence signal processing in the intact brain? Neocortical pyramidal neurons show slow oscillations (0.1–2 Hz) between up- and down-states separated by almost 20 mV, during slow wave sleep, quiet wakefulness, and under anesthesia (Petersen et al., 2003; Steriade et al., 1993). Depolarizations mimicking up- and down-states led to axonal AP broadening by ~40%, which we show can enhance synaptic strength at layer 5 synapses by on average 10% (up to 24%). Given that layer 5 neurons located in the same cortical column are highly interconnected (Markram et al., 1997) and that up-states are highly synchronized across neocortical pyramidal neurons (Petersen et al., 2003; Steriade et al., 1993), even a modest increase in layer 5 to layer 5 connection strength could have a profound impact on strengthening network coupling and synchronization in the cortex. The dependence of uEPSP facilitation on synapse location in the axonal arbor adds an additional level of spatial complexity that will favor synchronization of neurons connected by proximal synapses. Furthermore, the widespread expression of Kv1 channels in other excitatory (Guan et al., 2006) and inhibitory neurons in the neocortex (Wang et al., 2004), along with the prevalence of local connections formed by proximal presynaptic terminals in cortical areas (Binzegger et al., 2004), makes it likely that the findings described here will also apply to other intracortical connections. Indeed, there is evidence that Kv1 channels can also modulate inhibitory synaptic transmission in the cortex (van Brederode et al., 2001).

Finally, given the high metabolic cost associated with AP generation (Juusola and French, 1997; Laughlin and Sejnowski, 2003) and the strikingly sparse firing of cortical neurons in vivo (0.5 s^{-1}) (Lee et al., 2006; Manns et al., 2004), the ability to encode somatodendritic voltage signals via changes in the shape of the axonal AP waveform offers an economic means by which axons can enhance the computational capacity of neurons.

EXPERIMENTAL PROCEDURES

All experiments were carried out according to guidelines approved by the Animal Ethics Committee of the Australian National University. Male or female Wistar rats (2–5 weeks of age) were deeply anesthetized by isoflurane inhalation and quickly decapitated. One brain hemisphere was removed, and parasagittal brain slices (300 μm) were prepared from S1 cortex, including barrel, hind-, and forelimb areas. Throughout the slice preparation, the brain was maintained in ice-cold ACSF consisting of (in mM) 125 NaCl, 25 $NaHCO_3$, 3 KCl, 1.25 NaH_2PO_4, 25 glucose, 2 $CaCl_2$, and 7 $MgCl_2$ (pH 7.4; oxygenated with 95% O_2/5% CO_2). After cutting, slices were transferred to a holding chamber filled with oxygenated ACSF maintained at 35°C for 45 min and thereafter stored at room temperature.

Soma-Axon Recordings

During recording, individual slices were transferred to the stage of an upright microscope equipped with IR-DIC optics. The microscope bath was perfused with oxygenated (95% O_2, 5% CO_2) ACSF consisting of (in mM) 125 NaCl, 25 $NaHCO_3$, 3 KCl, 1.25 NaH_2PO_4, 25 glucose, 2 $CaCl_2$, and 1 $MgCl_2$. Dual or triple current-clamp whole-cell recordings were made from visualized layer 5 pyramidal neurons using identical Dagan BVC-700A amplifiers (Dagan Corporation, Minneapolis, MN). Whole-cell patch pipettes were made from borosilicate glass (Harvard, Edenbridge, Kent, UK) pulled to an open tip resistance of 5–6 MΩ (soma), 10 MΩ (axon blebs), and 12–15 MΩ (AIS). Pipettes were filled with (in mM) 100–120 K-gluconate, 20 KCl, 4 Mg-ATP, 0.3 Na-GTP, 10 HEPES, and 10 Na_2-phosphocreatine (pH 7.4 with KOH; osmolarity adjusted to 290 mOsmol with sucrose). Unless otherwise stated, all chemicals were obtained from Sigma-Aldrich (Sigma-Aldrich Inc., St. Louis, MO). All data were obtained at ~34°C. The axonal recording distances (hillock to recording site) were taken as linear estimations from the IR-DIC image field. Post hoc reconstructions of axons of biocytin-filled cells (2 mg ml^{-1}, e.g., Figure 5A) indicated a strong positive correlation with these estimations ($r^2 = 0.986$, $p < 0.001$, $n = 7$, data not shown) and slope close to 0.98. Action potentials were evoked by brief (2–3 ms) current injections (2–5 nA), and voltage was analog low-pass filtered at 10–30 kHz (Bessel) and digitally sampled at 50–100 kHz using an A-D converter (ITC-18, Instrutech) and data acquisition software Axograph (v. 4.9.1, Molecular Devices Corp., Sunnyvale, CA). Access resistance was on average ~20 MΩ for somatic recordings and 40 MΩ for axonal recordings and was fully compensated using bridge balance and capacitance neutralization. Recordings were aborted if the access resistance was >55 MΩ. All AP properties were determined from AP threshold, defined as the voltage at which the AP depolarization rate approximates 50 V s^{-1}. Time of AP onset was determined at the 50% onset time in a linear regression to the region of maximum slope of the AP. Local applications of 4-AP (100 μM in ACSF) or DTX-I (500 nM in ACSF) were performed via pressure application from a patch pipette using a Picospritzer system (Intracel, Herts), adjusting duration and pressure to obtain a localized response as determined from IR-DIC slice imaging (~50 μm radius; see Figure S3).

Paired Recordings

Paired recordings between layer 5 pyramidal neurons were performed as described (Kampa et al., 2006). Connectivity was assessed using trains of 5 APs at 20 Hz, and uEPSPs were recorded at low frequency (0.25 Hz). Paired-pulse ratio (PPR) was determined using alternating single and double presynaptic APs (25 ms interval). The amplitude of the second uEPSP was determined by subtracting the average uEPSP obtained during the single AP from that evoked by double APs. After 10 min of stable baseline recording, DTX-I (75–100 nM; Alomone labs, Israel) was bath applied for 7–20 min and characterized for up to 60 min

after drug application, during which time little if any washout was observed. To minimize the possibility of bath contamination with DTX-I due to its high affinity, we routinely used long periods of washing with high flow rates. Coefficient of variation analysis was performed as described (Faber and Korn, 1991). The standard deviation of uEPSP peaks was corrected for baseline noise. Local application of DTX-I (100 - 500 nM) was performed with a patch-pipette located in close proximity (<10 μm) of the distal AIS. DTX-I was dissolved in ACSF (95% O_2/5% CO_2) and continuously perfused with low pressure (~0.2 psi) to minimize spillover to nearby synaptic terminals. The effect of steady-state depolarization on uEPSP amplitude was assessed by depolarizing the presynaptic neuron to a just subthreshold membrane potential via somatic current injection for 8.5 s. APs were elicited by additional, brief current injections 75 ms, 2 s, and 8 s after the onset of the depolarization (see Figure 7). Episodes with depolarization were interleaved and compared to episodes without depolarization. In addition, episodes with single APs were interleaved with double APs (25 ms apart) to assess the paired-pulse ratio. These experiments were performed in connections where uEPSP amplitude was >0.5 mV to insure good signal-to-noise ratio. The incidence of significant unitary EPSP enhancement at 8 s was 80% for 2- to 3-week-old rats, but lower in older animals (17% for 3- to 5-week-old rats). In some of these experiments, biocytin (1–2 mg ml^{-1}; Sigma) was added to the intracellular solution for subsequent recovery of the morphology.

Voltage-Clamp Recordings

Cell-attached recordings of macroscopic K^+ currents used patch pipettes intracellularly filled with (in mM) 125 NaCl, 2.5 KCl, 10 HEPES, 10 glucose, 2 $CaCl_2$, 1 $MgCl_2$, 1 μM TTX, and 10 μM XE991 (pH 7.4, 285 mOsm). For outside-out or whole-cell voltage-clamp recordings, the intracellular solution contained (in mM) 120 K-methylsulfate, 15 KCl, 10 HEPES, 10 Na_2-phosphocreatine, 5 EGTA, 4 Mg-ATP, and 0.3 Na-GTP (pH 7.3, 280 mOsm). In addition, 2–10 μM XE991, 0.5 μM TTX, and 0.1% BSA were added to the extracellular ACSF. The presence of XE991 appeared crucial to remove slowly activating Kv7/KCNQ channels (M-current) (Wang et al., 1998), which are present in high densities in the distal AIS (Pan et al., 2006). Control experiments indicated that M-current activation did not play a role in regulating axonal or somatic AP duration or afterhyperpolarization (10 μM XE991 altered axonal AP duration and half-width by less than 2%, $p > 0.3$, $n = 3$). Voltage-clamp recordings were made with an Axopatch 200B amplifier (Molecular Devices Corp.). Cell-attached patch-clamp recordings were low-pass filtered at 2 kHz (8-pole Bessel) and sampled at 5 kHz. An on-line P/N (P/10) protocol was used to subtract leak and residual capacitive currents. The patch holding potential was estimated assuming a somatic resting membrane potential of −75 mV, which assumes full correction of the liquid junctions potential of ~14 mV in whole-cell current-clamp recordings (K-gluconate based). Membrane potentials for whole-cell and outside-out voltage-clamp recordings (K-methylsulfate based) were corrected for a −7 mV junction potential. Outside-out and/or whole-cell recordings were performed with 10 kHz low-pass filtering and 50 kHz sampling, and leak and capacitive currents subtracted with a P/4 protocol. All steady-state activation curves were constructed from peak currents after conversion to conductance assuming a K^+ reversal potential of −85 mV, were normalized to the maximum conductance, and fitted with a single Boltzmann equation (Figure 2C).

Histochemistry

For morphological reconstructions, 1–2 mg ml^{-1} biocytin (Sigma) was added to the intracellular solution. Immediately after recording, slices were fixed in 0.1 M phosphate-buffered saline (pH 7.4) containing 4% paraformaldehyde and 0.1% picric acid for 24 hr. Slices were afterward processed for biotinylated horseradish peroxidase conjugated to avidin (ABC-elite, Vectastain, Vector laboratories Inc., Burlingame, CA) according to previously published procedures (Horikawa and Armstrong, 1988) and mounted in Mowiol. Before processing, each slice was coded to enable blind morphometric analysis for a single unidirectional connection, used in the paired whole-cell experiments. Light-microscopic 3D computerized reconstructions were made with a Zeiss 63×/1.4 DIC oil-immersion objective and Neurolucida software (v.7, Microbrightfield Inc., Williston, VT). Previous work has indicated a high degree of correlation between light- or electron microscopy identification of synaptic contacts, with light microscopy tending to underestimate the number of contacts (Markram et al., 1997). Analysis of synaptic contact location included all pairs in which synapses could be unequivocally detected and was performed without prior knowledge of the outcome of the electrophysiological experiment.

Statistics

Statistical significance between groups was tested using paired or unpaired two-tailed Student's t tests using a cut-off significance level (p) of 0.05. In cases of multiple replicates for different time points, we analyzed the main effect with a repeated-measures two-way ANOVA. Correlation coefficients were determined using Pearson test (Prism 4.0, GraphPad Software Inc., San Diego, CA).

Supplemental Data

The Supplemental Data for this article can be found online at http://www.neuron.org/cgi/content/full/55/4/633/DC1/.

Received: February 18, 2007
Revised: June 4, 2007
Accepted: July 25, 2007
Published: August 15, 2007

REFERENCES

Alle, H., and Geiger, J.R. (2006). Combined analog and action potential coding in hippocampal mossy fibers. Science *311*, 1290–1293.

Awatramani, G.B., Price, G.D., and Trussell, L.O. (2005). Modulation of transmitter release by presynaptic resting potential and background calcium levels. Neuron *48*, 109–121.

Baccus, S.A. (1998). Synaptic facilitation by reflected action potentials: enhancement of transmission when nerve impulses reverse direction at axon branch points. Proc. Natl. Acad. Sci. USA *95*, 8345–8350.

Bekkers, J.M. (2000). Properties of voltage-gated potassium currents in nucleated patches from large layer 5 cortical pyramidal neurons of the rat. J. Physiol. *525*, 593–609.

Bekkers, J.M., and Delaney, A.J. (2001). Modulation of excitability by alpha-dendrotoxin-sensitive potassium channels in neocortical pyramidal neurons. J. Neurosci. *21*, 6553–6560.

Binzegger, T., Douglas, R.J., and Martin, K.A. (2004). A quantitative map of the circuit of cat primary visual cortex. J. Neurosci. *24*, 8441–8453.

Bischofberger, J., Geiger, J.R., and Jonas, P. (2002). Timing and efficacy of Ca2+ channel activation in hippocampal mossy fiber boutons. J. Neurosci. *22*, 10593–10602.

Borst, J.G., and Sakmann, B. (1999). Effect of changes in action potential shape on calcium currents and transmitter release in a calyx-type synapse of the rat auditory brainstem. Philos. Trans. R. Soc. Lond. B Biol. Sci. *354*, 347–355.

Byrne, J.H., and Kandel, E.R. (1996). Presynaptic facilitation revisited: state and time dependence. J. Neurosci. *16*, 425–435.

Chiu, S.Y., and Ritchie, J.M. (1981). Evidence for the presence of potassium channels in the paranodal region of acutely demyelinated mammalian single nerve fibres. J. Physiol. *313*, 415–437.

Cox, C.L., Denk, W., Tank, D.W., and Svoboda, K. (2000). Action potentials reliably invade axonal arbors of rat neocortical neurons. Proc. Natl. Acad. Sci. USA *97*, 9724–9728.

Debanne, D. (2004). Information processing in the axon. Nat. Rev. Neurosci. *5*, 304–316.

Debanne, D., Guerineau, N.C., Gahwiler, B.H., and Thompson, S.M. (1997). Action-potential propagation gated by an axonal I(A)-like K+ conductance in hippocampus. Nature *389*, 286–289.

Dodson, P.D., and Forsythe, I.D. (2004). Presynaptic K+ channels: electrifying regulators of synaptic terminal excitability. Trends Neurosci. *27*, 210–217.

Dodson, P.D., Billups, B., Rusznak, Z., Szucs, G., Barker, M.C., and Forsythe, I.D. (2003). Presynaptic rat Kv1.2 channels suppress synaptic terminal hyperexcitability following action potential invasion. J. Physiol. *550*, 27–33.

Faber, D.S., and Korn, H. (1991). Applicability of the coefficient of variation method for analyzing synaptic plasticity. Biophys. J. *60*, 1288–1294.

Geiger, J.R., and Jonas, P. (2000). Dynamic control of presynaptic Ca(2+) inflow by fast-inactivating K(+) channels in hippocampal mossy fiber boutons. Neuron *28*, 927–939.

Guan, D., Lee, J.C., Tkatch, T., Surmeier, D.J., Armstrong, W.E., and Foehring, R.C. (2006). Expression and biophysical properties of Kv1 channels in supragranular neocortical pyramidal neurones. J. Physiol. *571*, 371–389.

Harvey, A.L. (2001). Twenty years of dendrotoxins. Toxicon *39*, 15–26.

Horikawa, K., and Armstrong, W.E. (1988). A versatile means of intracellular labeling: injection of biocytin and its detection with avidin conjugates. J. Neurosci. Methods *25*, 1–11.

Inda, M.C., DeFelipe, J., and Munoz, A. (2006). Voltage-gated ion channels in the axon initial segment of human cortical pyramidal cells and their relationship with chandelier cells. Proc. Natl. Acad. Sci. USA *103*, 2920–2925.

Ishikawa, T., Nakamura, Y., Saitoh, N., Li, W.B., Iwasaki, S., and Takahashi, T. (2003). Distinct roles of Kv1 and Kv3 potassium channels at the calyx of Held presynaptic terminal. J. Neurosci. *23*, 10445–10453.

Jackson, M.B. (1993). Passive current flow and morphology in the terminal arborizations of the posterior pituitary. J. Neurophysiol. *69*, 692–702.

Jackson, M.B., Konnerth, A., and Augustine, G.J. (1991). Action potential broadening and frequency-dependent facilitation of calcium signals in pituitary nerve terminals. Proc. Natl. Acad. Sci. USA *88*, 380–384.

Juusola, M., and French, A.S. (1997). The efficiency of sensory information coding by mechanoreceptor neurons. Neuron *18*, 959–968.

Kampa, B.M., Letzkus, J.J., and Stuart, G.J. (2006). Cortical feed-forward networks for binding different streams of sensory information. Nat. Neurosci. *9*, 1472–1473.

Koester, H.J., and Sakmann, B. (2000). Calcium dynamics associated with action potentials in single nerve terminals of pyramidal cells in layer 2/3 of the young rat neocortex. J. Physiol. *529*, 625–646.

Kuba, H., Ishii, T.M., and Ohmori, H. (2006). Axonal site of spike initiation enhances auditory coincidence detection. Nature *444*, 1069–1072.

Laughlin, S.B., and Sejnowski, T.J. (2003). Communication in neuronal networks. Science *301*, 1870–1874.

Lee, A.K., Manns, I.D., Sakmann, B., and Brecht, M. (2006). Whole-cell recordings in freely moving rats. Neuron *51*, 399–407.

Manns, I.D., Sakmann, B., and Brecht, M. (2004). Sub- and suprathreshold receptive field properties of pyramidal neurones in layers 5A and 5B of rat somatosensory barrel cortex. J. Physiol. *556*, 601–622.

Manor, Y., Koch, C., and Segev, I. (1991). Effect of geometrical irregularities on propagation delay in axonal trees. Biophys. J. *60*, 1424–1437.

Markram, H., Lubke, J., Frotscher, M., Roth, A., and Sakmann, B. (1997). Physiology and anatomy of synaptic connections between thick tufted pyramidal neurones in the developing rat neocortex. J. Physiol. *500*, 409–440.

Palmer, L.M., and Stuart, G.J. (2006). Site of action potential initiation in layer 5 pyramidal neurons. J. Neurosci. *26*, 1854–1863.

Pan, Z., Kao, T., Horvath, Z., Lemos, J., Sul, J.Y., Cranstoun, S.D., Bennett, V., Scherer, S.S., and Cooper, E.C. (2006). A common ankyrin-G-based mechanism retains KCNQ and NaV channels at electrically active domains of the axon. J. Neurosci. *26*, 2599–2613.

Petersen, C.C., Hahn, T.T., Mehta, M., Grinvald, A., and Sakmann, B. (2003). Interaction of sensory responses with spontaneous depolarization in layer 2/3 barrel cortex. Proc. Natl. Acad. Sci. USA *100*, 13638–13643.

Rasband, M.N., and Shrager, P. (2000). Ion channel sequestration in central nervous system axons. J. Physiol. *525*, 63–73.

Rasband, M.N., Trimmer, J.S., Schwarz, T.L., Levinson, S.R., Ellisman, M.H., Schachner, M., and Shrager, P. (1998). Potassium channel distribution, clustering, and function in remyelinating rat axons. J. Neurosci. *18*, 36–47.

Robertson, B., Owen, D., Stow, J., Butler, C., and Newland, C. (1996). Novel effects of dendrotoxin homologues on subtypes of mammalian Kv1 potassium channels expressed in Xenopus oocytes. FEBS Lett. *383*, 26–30.

Schaefer, A.T., Helmstaedter, M., Schmitt, A.C., Bar-Yehuda, D., Almog, M., Ben-Porat, H., Sakmann, B., and Korngreen, A. (2007). Dendritic voltage-gated K+ conductance gradient in pyramidal neurones of neocortical layer 5B. J. Physiol. *579*, 737–752.

Shu, Y., Duque, A., Yu, Y., Haider, B., and McCormick, D.A. (2006a). Properties of action potential initiation in neocortical pyramidal cells: evidence from whole cell axon recordings. J. Neurophysiol. *97*, 746–760.

Shu, Y., Hasenstaub, A., Duque, A., Yu, Y., and McCormick, D.A. (2006b). Modulation of intracortical synaptic potentials by presynaptic somatic membrane potential. Nature *441*, 761–765.

Shu, Y., Yu, Y., Yang, J., and McCormick, D.A. (2007). Selective control of cortical axonal spikes by a slowly inactivating K+ current. Proc. Natl. Acad. Sci. USA *104*, 11453–11458.

Sloper, J.J., and Powell, T.P. (1979). A study of the axon initial segment and proximal axon of neurons in the primate motor and somatic sensory cortices. Philos. Trans. R. Soc. Lond. B Biol. Sci. *285*, 173–197.

Southan, A.P., and Robertson, B. (1998). Patch-clamp recordings from cerebellar basket cell bodies and their presynaptic terminals reveal an asymmetric distribution of voltage-gated potassium channels. J. Neurosci. *18*, 948–955.

Steriade, M., Nunez, A., and Amzica, F. (1993). A novel slow (< 1 Hz) oscillation of neocortical neurons in vivo: depolarizing and hyperpolarizing components. J. Neurosci. *13*, 3252–3265.

Storm, J.F. (1988). Temporal integration by a slowly inactivating K+ current in hippocampal neurons. Nature *336*, 379–381.

Stuart, G., Spruston, N., Sakmann, B., and Hausser, M. (1997). Action potential initiation and backpropagation in neurons of the mammalian CNS. Trends Neurosci. *20*, 125–131.

Stühmer, W., Ruppersberg, J.P., Schroter, K.H., Sakmann, B., Stocker, M., Giese, K.P., Perschke, A., Baumann, A., and Pongs, O. (1989). Molecular basis of functional diversity of voltage-gated potassium channels in mammalian brain. EMBO J. *8*, 3235–3244.

van Brederode, J.F., Rho, J.M., Cerne, R., Tempel, B.L., and Spain, W.J. (2001). Evidence of altered inhibition in layer V pyramidal neurons from neocortex of Kcna1-null mice. Neuroscience *103*, 921–929.

Van Wart, A., Trimmer, J.S., and Matthews, G. (2007). Polarized distribution of ion channels within microdomains of the axon initial segment. J. Comp. Neurol. *500*, 339–352.

Wang, H.S., Pan, Z., Shi, W., Brown, B.S., Wymore, R.S., Cohen, I.S., Dixon, J.E., and McKinnon, D. (1998). KCNQ2 and KCNQ3 potassium channel subunits: molecular correlates of the M-channel. Science *282*, 1890–1893.

Wang, Y., Toledo-Rodriguez, M., Gupta, A., Wu, C., Silberberg, G., Luo, J., and Markram, H. (2004). Anatomical, physiological and molecular properties of Martinotti cells in the somatosensory cortex of the juvenile rat. J. Physiol. *561*, 65–90.

Weller, U., Bernhardt, U., Siemen, D., Dreyer, F., Vogel, W., and Habermann, E. (1985). Electrophysiological and neurobiochemical evidence for the blockade of a potassium channel by dendrotoxin. Naunyn Schmiedebergs Arch. Pharmacol. *330*, 77–83.

Williams, S.R., and Stuart, G.J. (1999). Mechanisms and consequences of action potential burst firing in rat neocortical pyramidal neurons. J. Physiol. *521*, 467–482.

Williams, S.R., and Stuart, G.J. (2003). Role of dendritic synapse location in the control of action potential output. Trends Neurosci. *26*, 147–154.

Wolff, M., Vogel, W., and Safronov, B.V. (1998). Uneven distribution of K+ channels in soma, axon and dendrites of rat spinal neurones: functional role of the soma in generation of action potentials. J. Physiol. *509*, 767–776.